Research Article | Vol. 26, No. 3 | 5 Feb 2018 | OPTICS EXPRESS 2675

Optics EXPRESS

Suspended polarization beam splitter on silicon-on-insulator

CARLOS ERRANDO-HERRANZ,* SANDIPAN DAS, AND KRISTINN B. GYLFASON

Micro and Nanosystems, KTH Royal Institute of Technology, Stockholm, Sweden
**carloseh@kth.se*

Abstract: Polarization handling in suspended silicon photonics has the potential to enable new applications in fields such as optomechanics, photonic microelectromechanical systems, and mid-infrared photonics. In this work, we experimentally demonstrate a suspended polarization beam splitter on a silicon-on-insulator waveguide platform, based on an asymmetric directional coupler. Our device presents polarization extinction ratios above 10 and 15 dB, and insertion losses below 5 and 1 dB, for TM and TE polarized input, respectively, across a 40 nm wavelength range at 1550 nm, with a device length below 8 μm. These results make our suspended polarization beam splitter a promising building block for future systems based on polarization diversity suspended photonics.

OCIS codes: (130.3120) Integrated optics devices; (130.0130) Integrated optics; (250.5300) Photonic integrated circuits; (260.5430) Polarization; (130.5440) Polarization-selective devices; (230.1360) Beam splitters.

References and links

1. D. Dai, L. Liu, S. Gao, D.-X. Xu, and S. He, "Polarization management for silicon photonic integrated circuits," Laser Photonics Rev. **7**, 303–328 (2013).
2. J.-W. Hoste, S. Werquin, T. Claes, and P. Bienstman, "Conformational analysis of proteins with a dual polarisation silicon microring," Opt. Express **22**, 2807 (2014).
3. N. Matsuda, H. Le Jeannic, H. Fukuda, T. Tsuchizawa, W. J. Munro, K. Shimizu, K. Yamada, Y. Tokura, and H. Takesue, "A monolithically integrated polarization entangled photon pair source on a silicon chip," Sci. Rep. **2**, 817 (2012).
4. D. Dai, Z. Wang, and J. E. Bowers, "Ultrashort broadband polarization beam splitter based on an asymmetrical directional coupler," Opt. Lett. **36**, 2590 (2011).
5. J. Wang, D. Liang, Y. Tang, D. Dai, and J. E. Bowers, "Realization of an ultra-short silicon polarization beam splitter with an asymmetrical bent directional coupler," Opt. Lett. **38**, 4–6 (2013).
6. Y. Zhang, Y. He, J. Wu, X. Jiang, R. Liu, C. Qiu, X. Jiang, J. Yang, C. Tremblay, and Y. Su, "High-extinction-ratio silicon polarization beam splitter with tolerance to waveguide width and coupling length variations," Opt. Express **24**, 6586–6593 (2016).
7. S. Lin, J. Hu, and K. B. Crozier, "Ultracompact, broadband slot waveguide polarization splitter," APL **98**, 151101 (2011).
8. Z. Lu, Y. Wang, F. Zhang, N. A. F. Jaeger, and L. Chrostowski, "Wideband silicon photonic polarization beamsplitter based on point-symmetric cascaded broadband couplers," Opt. Express **23**, 29413–29422 (2015).
9. M. Aspelmeyer, T. J. Kippenberg, and F. Marquardt, "Cavity optomechanics," Rev. Mod. Phys. **86**, 1391–1452 (2014).
10. F. Chollet, "Devices Based on Co-Integrated MEMS Actuators and Optical Waveguide: A Review," Micromachines **7**, 18 (2016).
11. G. J. Veldhuis, O. Parriaux, H. J. W. M. Hoekstra, and P. V. Lambeck, "Sensitivity enhancement in evanescent optical waveguide sensors," J. Lightwave Technol. **18**, 677–682 (2000).
12. D. Marcuse, *Theory of Dielectric Optical Waveguides* (Elsevier, 1974).
13. T. Hu, B. Dong, X. Luo, T.-Y. Liow, J. Song, C. Lee, and G.-Q. Lo, "Silicon photonic platforms for mid-infrared applications [Invited]," Photonics Res. **5**, 417–430 (2017).
14. L. Fan, C.-L. Zou, M. Poot, R. Cheng, X. Guo, X. Han, and H. X. Tang, "Integrated optomechanical single-photon frequency shifter," Nat. Photonics **10**, 766–770 (2016).
15. M. Bagheri, M. Poot, M. Li, W. P. H. Pernice, and H. X. Tang, "Dynamic manipulation of nanomechanical resonators in the high-amplitude regime and non-volatile mechanical memory operation," Nat. Nanotechnol. **6**, 726–732 (2011).
16. E. A. Kittlaus, H. Shin, and P. T. Rakich, "Large Brillouin amplification in silicon," Nat. Photonics **10**, 463–467 (2016).
17. E. Verhagen and A. Alù, "Optomechanical nonreciprocity," Nat. Phys. **13**, 922–924 (2017).

#308741 https://doi.org/10.1364/OE.26.002675
Journal © 2018 Received 13 Oct 2017; revised 18 Jan 2018; accepted 18 Jan 2018; published 25 Jan 2018

18. A. H. Safavi-Naeini, S. Gröblacher, J. T. Hill, J. Chan, M. Aspelmeyer, and O. Painter, "Squeezed light from a silicon micromechanical resonator," Nature **500**, 185–189 (2013).
19. C. Errando-Herranz, F. Niklaus, G. Stemme, and K. B. Gylfason, "Low-power microelectromechanically tunable silicon photonic ring resonator add-drop filter," Opt. Lett. **40**, 3556–3559 (2015).
20. S. Han, T. J. Seok, N. Quack, B.-W. Yoo, and M. C. Wu, "Large-scale silicon photonic switches with movable directional couplers," Optica **2**, 370–375 (2015).
21. P. T. Lin, S. W. Kwok, H.-Y. G. Lin, V. Singh, L. C. Kimerling, G. M. Whitesides, and A. Agarwal, "Mid-Infrared Spectrometer Using Opto-Nanofluidic Slot-Waveguide for Label-Free On-Chip Chemical Sensing," Nano Lett. **14**, 231–238 (2014).
22. A. Vasiliev, A. Malik, M. Muneeb, B. Kuyken, R. Baets, and G. Roelkens, "On-Chip Mid-Infrared Photothermal Spectroscopy using Suspended Silicon-on-Insulator Microring Resonators," ACS Sensors **1**(11), 1301–1307 (2016).
23. Q. Xu, L. Chen, M. G. Wood, P. Sun, and R. M. Reano, "Electrically tunable optical polarization rotation on a silicon chip using Berry's phase," Nat. Commun. **5**, 5337 (2014).
24. A. P. Hope, T. G. Nguyen, A. Mitchell, and W. Bogaerts, "Quantitative Analysis of TM Lateral Leakage in Foundry Fabricated Silicon Rib Waveguides," IEEE Photonics Technol. Lett. **28**, 493–496 (2016).
25. D. Vermeulen, K. Acoleyen, S. Ghosh, S. Selvaraja, W. Cort, N. Yebo, E. Hallynck, K. Vos, P. Debackere, P. Dumon, W. Bogaerts, G. Roelkens, D. Thourhout, and R. Baets, "Efficient Tapering to the Fundamental Quasi-TM Mode in Asymmetrical Waveguides," "ECIO 2010 - European Conference on Integrated Optics," (2010).
26. S. Han, T. J. Seok, K. Yu, N. Quack, R. S. Muller, and M. C. Wu, "50x50 Polarization-Insensitive Silicon Photonic MEMS Switches: Design and Experiment," in "ECOC 2016 - Post Deadline Paper; 42nd European Conference on Optical Communication," (2016).
27. L. He, H. Li, and M. Li, "Optomechanical measurement of photon spin angular momentum and optical torque in integrated photonic devices," Sci. Adv. **2**, e1600485 (2016).

---

1. Introduction

Exploiting the polarization degree of freedom in silicon photonics has the potential to increase the bandwidth of optical communication systems [1], enable new sensors [2], and provide novel devices for polarization encoding in quantum information processing systems [3]. A key device required for such technology is the polarization beam splitter (PBS), which splits two orthogonal polarizations from one input waveguide into two different output waveguides [1,4–8].

Recently, devices based on suspended photonic waveguides have attracted significant attention, due to two fundamental aspects. First, suspended waveguides enable coupling between mechanical motion and optical fields, which leads to devices based on optically-induced motion, so-called optomechanics [9], and motion-induced optical tuning, generally called photonic microelectromechanical systems (MEMS) [10]. Second, the suspended solid core can be made very thin, and thus a large fraction of the optical power can propagate outside of the core and be used for sensing of gases or liquids, since suspended waveguides have a perfectly symmetric index difference between the core and the top and bottom claddings [11,12]. This is particularly interesting for mid-infrared (mid-IR) wavelengths, since the rotational and vibrational absorption lines of many relevant materials lie in the mid-IR [13].

Consequently, by using suspended photonic waveguides, new applications such as optical frequency conversion [14], optical memories [15], silicon lasers and amplifiers based on Brillouin scattering [16], non-reciprocal photonics [17], squeezed light generation [18], tunable and reconfigurable optical networks [19,20], and spectroscopy [21,22] have recently been demonstrated. For all these applications, the ability to handle both polarizations in the same chip brings new possibilities, e.g. in the form of greater bandwidth and/or resistance to disturbances [23].

While on-chip polarization beam splitting in suspended silicon photonics can be solved by using standard non-suspended PBS [23], this solution usually involves waveguide transitions between a suspended geometry and a non-suspended one. These transitions adversely affect the system performance, due to increased waveguide length and unwanted mode conversions that lead to increased optical losses, reflections, and interference [24,25]. Moreover, combining suspended waveguides with the standard oxide-clad waveguides in which PBS have traditionally been demonstrated involves additional fabrication steps, which complicates the fabrication process. Consequently, a suspended PBS that can be seamlessly integrated in a suspended silicon photonics platform is a key element to enable polarization diversity schemes. However, the required suspended PBS has, to our knowledge, not yet been demonstrated in any platform. In addition, such a device can potentially be combined with MEMS actuators to actively compensate for fabrication variations in critical features such as the coupling gap.

In this work, we design and experimentally demonstrate a suspended PBS, based on a standard silicon-on-insulator waveguide platform. Our suspended PBS features polarization extinction ratios (PER) above 10 and 15 dB, and insertion losses (IL) below 5 and 1 dB, for TM and TE polarized input, respectively, over a 40 nm wavelength range at 1550 nm, with a device length below 8 µm. These performance metrics are on par with state of the art of non-suspended PBS devices [1].

2. Design

Our suspended PBS is based on an asymmetric directional coupler formed by a strip waveguide coupled to a slot-waveguide [4, 7]. The large birefringence of these waveguides enables the design of a directional coupler that is phase matched only for one of the waveguide polarizations, and mismatched for the other. This results in a complete transfer of the power in the matched mode in a short propagation length, while the mismatched mode is unaffected. Using a slot-waveguide for the coupling region eases the achievement of quasi-transverse-magnetic (TM) mode matching, while ensuring a large quasi-transverse-electric (TE) mode mismatch, due to the significant fraction of the TE mode power propagating in the air-filled slot region, and the TE mode thus having a much lower effective mode index than its strip-waveguide counterpart.

Eigenmode simulations of TE and TM waveguide modes using COMSOL Multiphysics, shown in Fig. 1(a) and (b), show the effective mode indexes of strip and slot-waveguides with varying core widths. The height of the waveguides is chosen 220 nm, the silicon photonics de facto standard, with only a single mode confined in the vertical direction (and thus, we will from now on refer to our waveguide modes by a single index, e.g. TE_0). Here, we choose a strip waveguide width of 500 nm, and match its TM_0 mode index to a slot waveguide of 330 nm width, thus achieving mode matching for TM_0 while maintaining a large mode mismatch of 0.5 for the TE_0 modes. Note that we choose a slot-waveguide gap and a coupling gap of 100 nm and 150 nm, respectively, which allow for fabrication by deep-UV lithography.

Having fulfilled the mode matching requirement, the next step is to determine the coupling length for complete TM mode transfer. A first estimate can be obtained by simulating the eigenmodes of the coupled-waveguide system and extracting the effective mode indexes of its two TM supermodes, which are the modes that interact along the coupler and determine the power distribution along its length. Using the simulated effective supermode indexes n_{TM_0} and n_{TM_1}, the coupling length for full TM mode transfer can be estimated from coupled-mode theory [4] as

$$L_\pi = \frac{\lambda}{2(n_{\mathrm{TM}_0} - n_{\mathrm{TM}_1})} = \frac{1.55\ \mu\mathrm{m}}{2 \times (1.2952 - 1.1121)} = 4.23\ \mu\mathrm{m}. \tag{1}$$

Using this coupling length estimate as a first approximation, an optimization based on a three-dimensional finite difference time domain simulation (3D FDTD) using CST Microwave Studio was performed. This simulation takes other significant effects into account, not taken care of by the eigenmode estimate, such as the input and output waveguides. In particular, the output waveguide bend for the TE output, with chosen radius of 5 µm, increases significantly the effective coupling length for the TM mode. This optimization thus leads to the results in Fig. 2, and a nominal coupler length as short as 2.4 µm. From this simulation, one can also extract the significant figures of merit for the PBS, such as a polarization extinction ratio (PER) above 10 dB, and an insertion loss (IL) below 1 dB, for a wavelength range larger than 60 nm around 1550 nm (solid lines in Fig. 2(d) and (e)). It is important to note that the device is designed as a TM mode

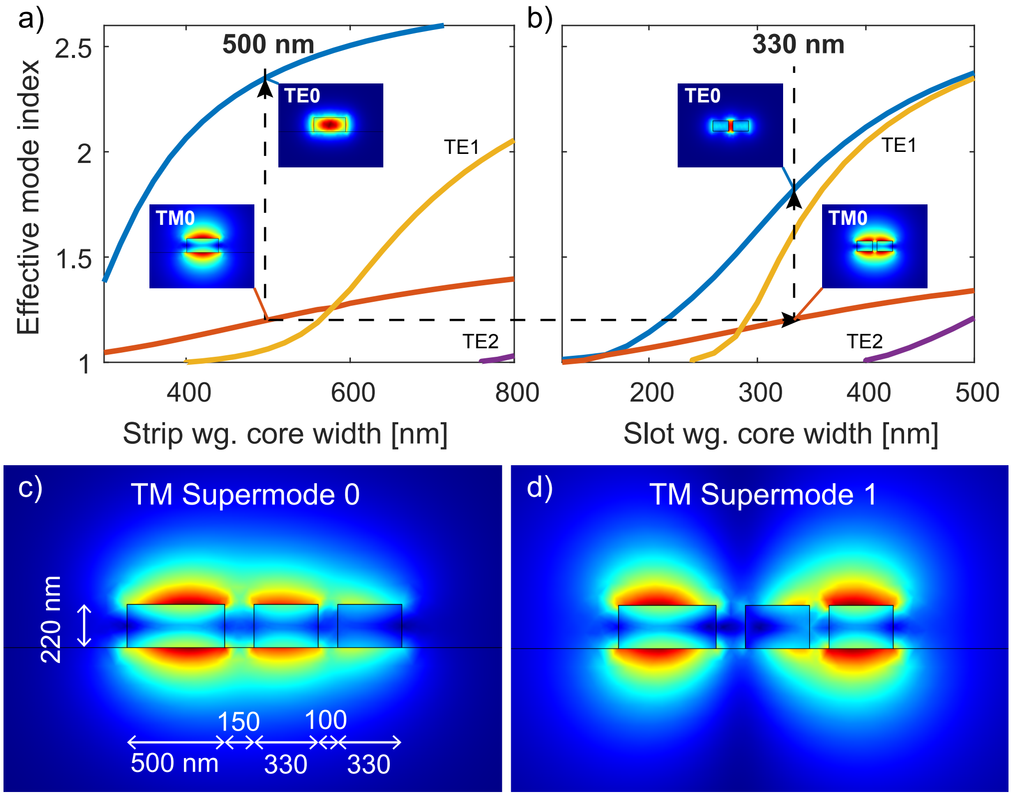

Fig. 1. Effective mode index extracted from waveguide eigenmode simulations for a) a strip- and b) a slot-waveguide with varying silicon core widths. A width of 500 nm and 330 nm are chosen to satisfy the mode matching condition for TM_0 while providing a large enough mode mismatch for the TE_0 modes (> 0.5). c) and d) show the two TM supermodes present in the coupled-waveguide system, which interact along the device and result in TM_0 mode coupling while leaving the TE_0 mode intact. All the geometrical parameters in c) and d) are in units of nm.

directional coupler, which limits the bandwidth for the TM mode (Fig. 2(c)) while leaving the TE mode mostly unaffected, as shown in the FDTD simulation results in Fig. 2(b).

Moreover, we simulated the effects of variations in two critical parameters of the coupler: the width of the slot-waveguide slot Δw_{slot}, and the width of the coupling gap $\Delta w_{coupler}$. Figure 2(d) shows the effect of a variation of ±40 nm in slot width, resulting in a 3 dB decrease in PER and a 1 dB increase in IL for an increased slot width, and 5 dB larger PER and 0.3 dB lower IL for a decreased slot width. Figure 2(e) shows the effect of a variation of ±40 nm in coupling gap, both cases resulting in a 3 dB decrease in PER and a 0.5 dB increase in IL.

3. Fabrication

Our fabrication followed the process reported in [19], and consisted of two electron beam lithography-defined silicon dry etching steps, which resulted in waveguides of 220 nm height, and a partially etched silicon slab of 110 nm. Through-etched parts of the design were subsequently underetched using a 50% solution of hydrofluoric acid (HF). The chip was then dried by critical-point drying (CPD), to avoid collapse and stiction of the suspended structures due to capillary forces during the drying process.

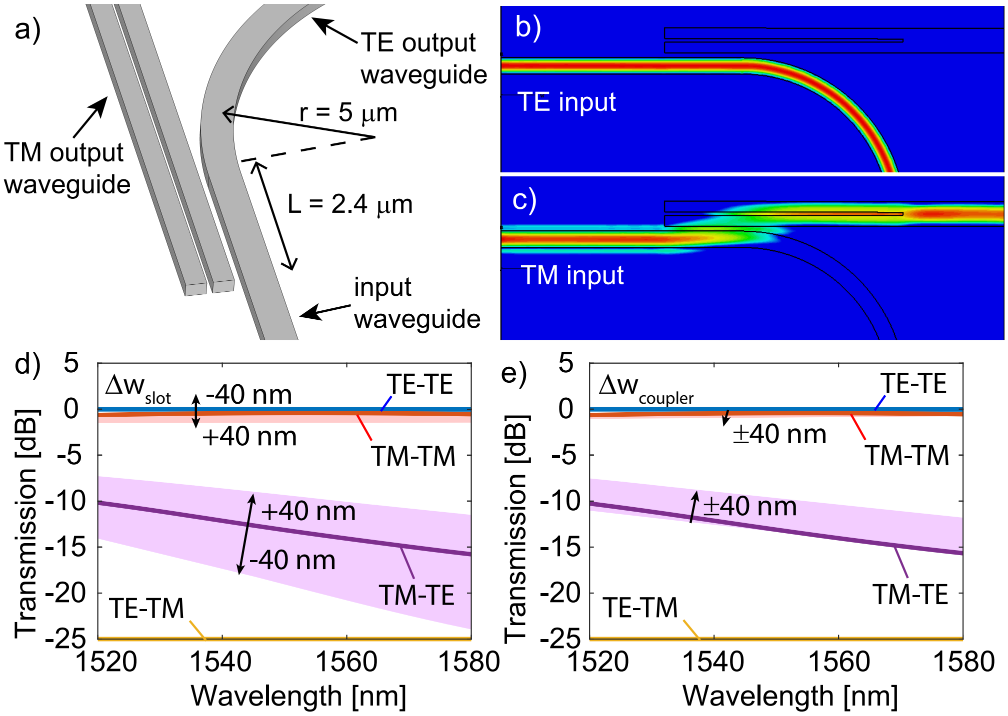

Fig. 2. a) The geometry of the 3D FDTD simulations, and b) top view of the simulated device routing the light to the bottom waveguide under TE-polarized input light, and c) routing the light to the top waveguide under TM-polarized input light. d) Solid lines show the transmission results, yielding a PER above 10 dB and an IL for TM below 1 dB for a 60 nm range at 1550 nm, for our designed values. The shaded areas show the effect of a fabrication variations in slot-waveguide slot width, and e) in the coupling gap.

Figure 3(a) shows optical microscope images of one set of two devices, with cross-sectional schematics showing significant structures. To evaluate our PBS design, we fabricated two devices, each with an input grating coupler designed for either TE or TM polarization transmission, followed by an adiabatic taper from 12 μm down to 500 nm width, and two output systems of the same adiabatic taper and a grating coupler each. The suspended PBS is supported by clamping regions at both ends. For the waveguides in which only TE polarization is transmitted, the clamping is based on tapering a section of 110 nm thick silicon slab. However, all our TM-transmitting waveguides were suspended via clamping beams on the sides of the input and output tapering sections. This is due to two causes: i) the low confinement of the TM mode in our waveguides, which results in mode leakage when close to the 110 nm silicon slab [24], and ii) the potential for mode conversions from TM$_0$ to TE$_1$ in vertically asymmetric tapers, which results in interference and losses [25]. Figure 3(b) shows a close-up scanning electron microscope (SEM) view of one PBS. We measured the waveguide and slot widths of three copies of our fabricated PBS design, yielding (mean ± standard deviation) strip waveguide width 513 ± 18 nm, slot waveguide beam widths 321 ± 5 and 335 ± 4 nm, slot width 91 ± 5 nm, and coupling gap 134 ± 5 nm.

4. Results and discussion

Light from a tunable laser with a central wavelength of 1550 nm and 1 mW output power was coupled into the chip through a 3-paddle fiber polarization controller connected to a cleaved

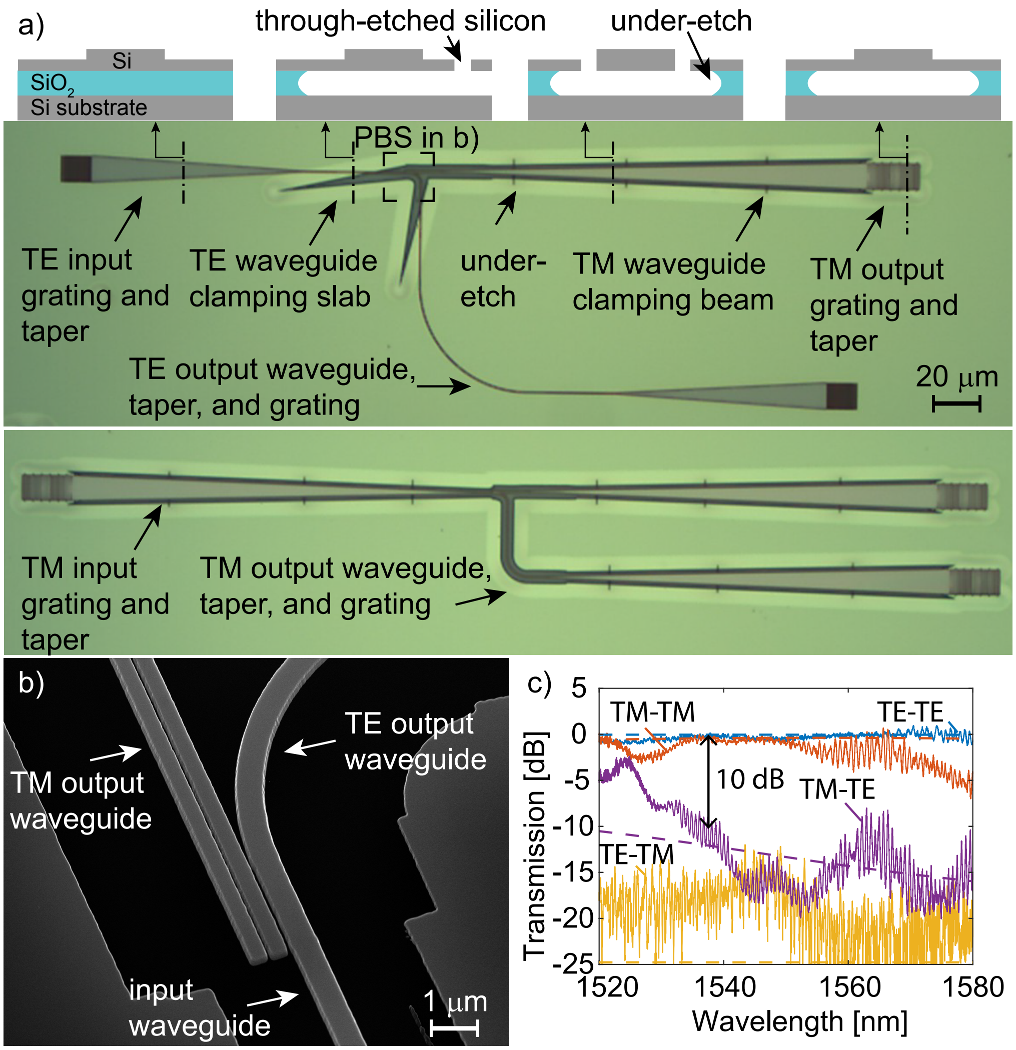

Fig. 3. a) Optical microscope images of a set of devices, with cross-sectional schematics. Our TE input device comprises a TE grating coupler input, our suspended PBS, and two outputs with their respective TM and TE grating couplers. Our TM input device consists of a TM input grating coupler and two TM output couplers b) Shows a magnified image of our PBS, showing the input waveguide, coupling region, and output waveguides. c) Normalized transmission measurements for the devices in a) show PER above 10 and 15 dB, and IL below 5 and 1 dB, for TM and TE polarized input light, respectively, across a 40 nm bandwidth at 1550 nm wavelength. Dashed lines represent the simulated transmission for the measured geometry of the device.

single-mode optical fiber, placed with a 10 degree vertical tilt on a 3-axis translational stage. The light was then coupled out of the chip and into a synchronized wavelength domain component analyzer via the two output couplers by another optical fiber, also tilted 10 degrees.

Figure 3(c) shows our normalized optical transmission measurements, overlaid with our simulated transmission for the measured fabricated geometry (dashed lines). We normalized our measurements using two reference devices, one for TE input PBS and one for TM input PBS to eliminate the contribution of the gratings and tapers on the measured PER, IL, and bandwidth of the PBS (only assuming negligible polarization rotation). The reference devices for TE input PBS consisted of i) input and output TE gratings (PER 15 dB), tapers, and connecting waveguide, and ii) input TE and output TM gratings (PER 5 dB), tapers, and waveguide, serving as references for i) TE and ii) TM grating output. Both arms of the TM input PBS were then normalized by a reference device consisting of input and output TM gratings with a 12 μm wide waveguide. The wider reference waveguide for TM is due to the presence of strong interference in tapered TM references, which we believe comes from a TM_0 to TE_1 conversion along the waveguide tapers, already reported in the literature [25]. The converted light is filtered out in the structures that contain a suspended PBS, but remains guided in the straight reference waveguide, and results in strong interference in the grating output of the reference waveguide. Our choice of a non-tapered TM reference results in an underestimated bandwidth and an overestimated IL for TM input to our PBS, which also includes the unknown TM tapering losses. For TM-polarized input, our devices show a PER above 10 dB and an IL below 5 dB over a bandwidth of 40 nm. For TE polarized input, a PER above 15 dB and an IL below 1 dB were measured across a bandwidth above 80 nm.

Our fabricated device features a deviation from designed values of -10 nm in slot width, which, in the light of our simulated values, increases the PER and decreases the IL. However, a decrease in 15 nm in coupling gap decreases PER and increases IL (See Fig. 2(c) and (d)), yielding roughly the designed transmission parameters(see dashed curves in Fig. 3(c)).

Our measured results, with PER above 10 and 15 dB, and IL below 5 and 1 dB, for TM and TE polarized input, respectively, over a 40 nm wavelength range at 1550 nm, and a short device length below 8 μm, are comparable to the performance of current state-of-the-art non-suspended PBS devices [1]. Our results, in combination with the completely suspended geometry, make our device an excellent candidate for PBS in suspended photonics, without requiring lossy waveguide transitions or increased complexity in the fabrication process. Consequently, our device can be useful for applications such as on-chip polarization beam splitting in polarization-insensitive photonic MEMS switches [26] or in dual-polarization optomechanics [27].

5. Conclusion

We have experimentally demonstrated, to the best of our knowledge, the first suspended PBS. Our device features polarization extinction ratios above 10 and 15 dB, and insertion losses below 5 and 1 dB, for TM and TE polarized input, respectively, over a 40 nm wavelength range at the telecom wavelength of 1550 nm, and a short device length below 8 μm. We believe that the presented device is a valuable building block for polarization handling in suspended silicon photonic systems, with applications in optical communications, quantum information processing, and sensing.

Funding

Swedish Research Council (621-2012-5364).

Acknowledgments

The authors thank Dr. Xi Chen and Dr. Lech Wosinski at the KTH ICT school for help with the characterization setup.